Published in final edited form as:

Mol Cancer Res. 2023 August 01; 21(8): 836–848. doi:10.1158/1541-7786.MCR-22-0763.

Desmoglein 2 Functions As A Receptor for Fatty Acid Binding Protein 4 in Breast Cancer Epithelial Cells

Dongmei Chen[1], **Keith M. Wirth**[2], **Scott Kizy**[2], **Joseph M. Muretta**[1], **Todd W Markowski**[1], **Peter Yong**[1], **Adam Sheka**[2], **Hisham Abdelwahab**[2,4], **Ann V. Hertzel**[1], **Sayeed Ikramuddin**[2], **Masato Yamamoto**[2,5], **David A Bernlohr**[1,3]

[1]Department of Biochemistry, Molecular Biology and Biophysics, The University of Minnesota-Twin Cities, Minneapolis, MN USA

[2]Department of Surgery, The University of Minnesota-Twin Cities, Minneapolis, MN USA

[5]Department of Masonic Cancer Center, The University of Minnesota-Twin Cities, Minneapolis, MN USA

Abstract

Fatty acid binding protein 4 (FABP4) is a secreted adipokine linked to obesity and progression of a variety of cancers. Obesity increases extracellular FABP4 (eFABP4) levels in animal models and in obese breast cancer patients compared to lean healthy controls. Using MCF-7 and T47D breast cancer epithelial cells, we show herein that eFABP4 stimulates cellular proliferation in a time and concentration dependent manner while the non-fatty acid-binding mutant, R126Q, failed to potentiate growth. When E0771 murine breast cancer cells were injected into mice, FABP4 null animals exhibited delayed tumor growth and enhanced survival compared to injections into control C57Bl/6J animals. eFABP4 treatment of MCF-7 cells resulted in a significant increase in phosphorylation of extracellular signal-regulated kinase 1/2 (pERK), transcriptional activation of nuclear factor E2-related factor 2 (NRF2) and corresponding gene targets ALDH1A1, CYP1A1, HMOX1, SOD1 and decreased oxidative stress, while R126Q treatment did not show any effects. Proximity-labeling employing an APEX2-FABP4 fusion protein revealed several proteins functioning in desmosomes as eFABP4 receptor candidates including desmoglein, desmocollin, junction plankoglobin, desomoplankin and cytokeratins. AlphaFold modeling predicted an interaction between eFABP4, and the extracellular cadherin repeats of DSG2 and pull-down and immunoprecipitation assays confirmed complex formation that was potentiated by oleic acid. Silencing of Desmoglein 2 in MCF-7 cells attenuated eFABP4 effects on cellular proliferation, pERK levels, and ALDH1A1 expression compared to controls.

Keywords

FABP4; Breast Cancer; Proliferation; Desmosome; Fatty Acid

[3]Author to whom correspondence should be addressed at: Department of Biochemistry, Molecular Biology and Biophysics, The University of Minnesota-Twin Cities, Bernl001@umn.edu, 612-624-2712.

[4]Current address: Weil Cornell Medicine-Qatar, Doha Qatar

Each author declares no potential conflicts of interest

INTRODUCTION

Whereas obesity has long been appreciated as a driver of metabolic disease, more recently, obesity has been implicated in the pathogenesis of a variety of cancers, particularly breast and pancreatic cancer [1]. The diagnosis of obesity is associated with a higher risk of diagnosis of breast cancer, higher risk of advanced disease at diagnosis, and increased hazard of death after diagnosis [2, 3]. Additionally, indicators of worsened metabolic disease, such as type II diabetes mellitus and metabolic syndrome, have demonstrated similar adverse relationships with breast cancer outcomes [4]. Whereas a number of potential mechanisms have been proposed that link adipose tissue to cancer (e.g., changes in adipokine secretion, fatty acids as fuels for cancer growth, increased local inflammation potentiated by tumor necrosis factor α and interleukin-6, none have been conclusive [1].

In search of a mechanistic link between obesity, metabolic disease, and cancer, fatty acid binding protein 4 (FABP4), alternatively called adipocyte protein 2 (aP2), has been suggested as a molecule of interest [5]. FABP4 is a small, 15-kDa fatty acid carrier protein predominantly expressed by adipocytes, but also found at low levels in macrophages and some endothelial cells. In adipocytes is involved in intracellular fatty acid trafficking and functions to mediate lipolysis [6] while in macrophages, it regulates fatty acid metabolism and leukotriene synthesis [7]. In response to lipolytic stimuli, FABP4 is secreted by adipocytes via a non-canonical mechanism linked to activation of SirT1 and autophagy [8]. Elevated circulating FABP4 levels have been linked to obesity [9], type 2 diabetes [10, 11], cardiovascular diseases [12–15], and allergic asthma [16]. Conversely, loss or inhibition of FABP4 exhibits reduced risk of coronary disease and type 2 diabetes [17–19], and protection from inflammation-related disorders [16, 17, 20]. FABP4 has also been implicated in the development and progression of a number of obesity related cancers [5]. Women with breast cancer demonstrate higher circulating serum levels of FABP4 and higher FABP4 expression levels in the breast stroma, as compared to healthy controls [21, 22]. Higher expression of FABP4 in breast cancer specimens is also significantly correlated with recurrence and disease-free survival [23]. Additionally, tumor progression is significantly decreased in FABP4 knockout models [22, 24].

The recent discovery of extracellular FABP4 (eFABP4) provided new insight into a role for FABP4 as an adipose-derived cytokine (adipokine) [25]. eFABP4 has been shown to regulate glucose synthesis in hepatocytes [25] and release of insulin from pancreatic β-cells [26]. In human umbilical vein endothelial cells (HUVECs), eFABP4 exhibited pro-oxidative and pro-inflammatory effects [27] while in cardiomyocytes, eFABP4 increased intracellular lipid accumulation that led to impairment of the insulin signaling and reduced insulin-stimulated glucose uptake [28]. In cancer cells, studies have described increased proliferation, invasiveness, and stemness of cancer cells in response to eFABP4 treatment [22, 29]. Potential mechanisms have implicated IL-6/Stat-3 dependent pathways, regulation of aldehyde dehydrogenase, FoxM1 pathways, and altered fatty acid metabolism [22, 24, 30]. These results suggest a model where eFABP4 binds to cell surface protein(s) to mediate cellular uptake and/or intracellular signaling. Herein, we present results suggesting eFABP4 binds to the extracellular domain of desmosomal proteins to mediate breast cancer epithelial cell growth via an ERK-NRF2 axis.

METHODS

Animal Care and Use

All experimental procedures using animals were reviewed and approved by the University of Minnesota Institutional Animal Care and Use Committee. Male C57BL/6J wild type (WT) and whole body FABP4 null (AKO) mice were fed ad libitum a high-saturated-fat (lard) diet (F3282; BioServe, Flemington, NJ) for 12 weeks after weaning. At week 12–14 of high fat diet, mice were injected with E0771 cells (5×10^6) in the mammary fat pads. Tumor volume was measured three times weekly with calipers. Mice were euthanized at endpoints of >2 cm^3, tumor ulceration, metastases or the end of study period at 35 days.

Cell Culture and Proliferation and Viability Analysis

MCF-7, E0771 and T47D were purchased from the American Tissue Culture Collection (ATCC; Manassas, VA) and all cells were quality assured to be mycoplasma free and verified. MCF-7 breast cancer cells and E0771 murine breast cancer cells were cultured in Dulbecco's modified Eagle's medium (DMEM) supplemented with 5% fetal bovine serum (FBS), 2 μg/mL insulin and 1 mM penicillin-streptomycin in a humidified incubator at 37° C with 5% CO_2. T47D cell lines were maintained in RPMI (Invitrogen) with 5% FBS and 2 μg/mL insulin. To assess the effect of FABP4 on cell growth, cells were seeded in 6-well plates at a concentration of 2×10^5 cells/mL in media containing 5% FBS and 2 μg/mL insulin. Cells were cultured for 24 hours, and baseline cell number determined utilizing an automated cell counter (Countess, Thermo Fisher) or CyQUANT cell proliferation assay kit (C7027, Invitrogen) according to the manufacturer's protocol. Media was aspirated and cells were washed with PBS. Cells were treated with 20–200 ng/mL eFABP4, R126Q, FABP5, 20 nM brusatol, or vehicle in media containing 0.1% FBS and 2 μg/mL insulin. Cell counting was determined at 24 or 48 hours post addition.

Cellular viability was determined using the LIVE/DEAD Viability/Cytotoxicity Kit (L3224, Invitrogen) according to the manufacturer's protocol. Viability or toxicity were determined using the two-indicator method where the ratio of fluorescence of calcein AM (excitation/emission ~495 nm/~515 nm) to ethidium homodimer-1 (EthD-1, (excitation/emission ~495 nm/~635 nm) was determined and compared between control and eFABP4 treated cells.

NRF2 Reporter Assays

The antioxidant response element (ARE) luciferase reporter vector and constitutively active Renilla luciferase vector (BPS Bioscience) were transfected into MCF-7 cells utilizing Lipofectamine (Invitrogen). After 24 hours, the media was aspirated and replaced with media containing 100 ng/mL FABP4. After 24 hours of incubation, dual luciferase reporter assay (Promega) was performed utilizing a luminometer per the manufacturer's instructions and ARE reporter activity was normalized to Renilla activity.

H_2O_2 Assay

Hydrogen peroxide (H_2O_2) quantification was determined using the Amplex Red hydrogen peroxide/peroxidase assay kit (A22188, Invitrogen) according to the manufacturer's protocol with modification. Briefly, cells were scraped into phosphate buffered saline pH 7.4 and

inactivated at 95° C for 10 min. After removal of cell debris, 50 μL of extract was incubated with 50 μL of substrate solution for 30 minutes and the fluorescence was measured using a microplate reader with excitation at 540 nm and emission at 590 nm.

Quantitative RT-PCR

Total RNA was isolated using TRIzol reagent (Invitrogen, Carlsbad, CA). cDNA synthesis was performed by using iScript (Bio-Rad, Hercules, CA) according to the manufacturer's protocol. Quantitative reverse transcription (qRT)-PCR amplification utilized a Bio-Rad CFX 96 real-time system with SYBR green Supermix. TATA-binding protein (TBP) was used as an internal control to normalize expression. The primer sequences were ALDH1A1 forward: CTTACCTGTCCTACTCACCGATTTG, ALDH1A1 reverse: TCCTTATCTCCTTCTTCTACCTGGC; CYP1A1 forward: GATTGAGCACTGTCAGGAGAAGC, CYP1A1 reverse: ATGAGGCTCCAGGAGATAGCAG; SOD1 forward: CTCACTCTCAGGAGACCATTGC, SOD1 reverse CCACAAGCCAAACGACTTCCAG; HMOX1 forward: CCAGGCAGAGAATGCTGAGTTC, HMOX1 reverse: AAGACTGGGCTCTCCTTGTTGC; TBP forward: AGCGGTTTGCTGCGGTAATC, TBP reverse: ACTGTTCTTCACTCTTGGCTCCTG, DSG2 forward: AGGGAAGCACAGCATGACTCCT, DSG2 reverse: CCTTTCCGCAATGGCACATCAG; DSC1 forward: CAGAGTCAAGATGGCTTCCCAG DSC1 reverse: GTTCTCAAGTCGCCAGTGTGTTG; DSC2 forward: CACAGAAGCTCCTGGAGATGAC, DSC2 reverse: GATGGTCTCCTGACCTCCGTTT. CYP1A1, SOD1, HMOX1, DSG2, DSC1 and DSC2 primers were from ORiGENE.

Generation of Recombinant Proteins

The ascorbate peroxidase 2 (APEX2) cDNA was obtained from Addgene (Plasmid #49386) and the APEX2-FABP4 and APEX2 sequences modified to contain unique restriction sites permissive for insertion were obtained by commercial gene synthesis and subcloned into pRSET-A vector (#3990, Addgene) and transformed into DH5α E. coli. Sequence verified clones were transformed into E. coli BL21(DE3)-pLysS for expression. Recombinant FABP isoforms (FABP4, R126Q FABP4, or FABP1) were expressed in E. coli as N-terminal His-tagged or GST-tagged fusion proteins as previously described (31). His-tagged recombinant proteins were purified using Ni^{+2} affinity chromatography while GST-tagged proteins were purified using glutathione-sepharose chromatography. Each recombinant protein was delipidated using Lipidex-1000 resin and stored at −80° C until use.

1,8-ANS binding Assay

To measure the binding affinity of recombinant proteins for fatty acids, the 1-anilinonaphthalene 8-sulfonic acid (1,8-ANS) binding assay was utilized as previously described (32). Briefly, a fixed concentration of FABP4, APEX2, or APEX2-FABP4 (10 μM) in assay buffer (20 mM Tris-HCl, 50 mM NaCl, 2 mM dithiothreitol, pH 7.4) was mixed with 1,8-ANS for 30 minutes at room temperature and the fluorescence intensity recorded using an excitation wavelength of 370 nm and emission wavelength of 470 nm.

In Vitro Peroxidase Activity

To evaluate the peroxidase activity of APEX2 and APEX2-FABP4, 3 pmol of recombinant proteins were mixed with peroxidase substrate (#34094, Thermo Fisher Scientific) for 10 minutes at room temperature and then spotted on nitrocellulose membrane for chemiluminescence detection.

Affinity Capture of Proximity-labeled Proteins

The culture media from MCF-7 cells at 70%–80% confluence was aspirated and 500 μM biotin-SS-tyramide (#914916, Sigma) pre-mixed with fresh growth media was added. After 15 minutes, cells were treated with 500 nM recombinant APEX2 or APEX2-FABP4 for 10 minutes at which time 1 mM H_2O_2 was supplied for 1 min to initiate oxidation and biotinylation of target proteins. The reaction was terminated by the addition of quench buffer (10 mM sodium azide, 10 mM sodium ascorbate, and 5 mM Trolox in phosphate-buffered saline) and cells immediately washed 3 times with phosphate-buffered saline and lysed (8M Urea, 0.4M Tris pH 8.0, 20% acetonitrile supplemented with protease inhibitors). Lysates were sonicated and centrifuged at 14 000 rpm for 10 min at 4° C. The bicinchoninic acid (BCA) assay was used to determine the protein content. To capture the biotinylated proteins, Streptavidin Magnetic Beads (#88817, Thermo Fisher Scientific) were pre-washed 6 times (2 times with phosphate buffered saline, one time with 1M KCl, one time with 0.1M Na_2CO_3, 1.6M Urea, 80mM Tris pH 8.0, 4% acetonitrile, and 2 times with phosphate buffered saline). Lysates were diluted 5-fold with phosphate buffered saline plus protease inhibitors and incubated with pre-washed beads overnight at 4° C. After capture, beads were washed 6 times and proteins eluted in 200 μL 50 mM Tris pH 8.0, 1.5 M Urea and 20 mM dithiothreitol at room temperature for 0.5 hours. The elution and pull-down steps were repeated three times and the eluates pooled for mass spectrometry analysis.

Mass Spectrometry Analysis

For each sample, 5 μg was incubated with 50 mM chloroacetamide in 50 mM ammonium bicarbonate and incubated at room temperature for 15 min. Following modification, trypsin was added to each sample and incubated at 37° C overnight. The resultant peptides were desalted using an MCX stage tip (https://doi.org/10.1021/ac026117i) and eluted sequentially using 5% trifluoroacetic acid followed by 50% acetonitrile in water (v/v) and finally 100% acetonitrile. Peptides were dried and reconstituted in sample buffer (97.99:2:0.01, water:acetonitrile:formic acid) and analyzed on an Orbitrap Fusion (Thermo Scientific, Waltham, MA) liquid chromatography-mass spectrometry system in data dependent acquisition mode. Data was collected from 15 dependent scans on the Orbitrap Fusion.

The MS/MS data was then analyzed using Sequest (Thermo Scientific in Proteome Discoverer 2.4.0305) and the human Universal Proteome UP0000005640 protein sequence database with canonical sequence as the target after concatenation with the common lab contaminants protein sequences as per https://www.thegpm.org/crap/. Scaffold (version 4.11, Proteome Software Inc., Portland, OR) was used to validate MS/MS based peptide and protein identifications reported by Sequest.

AlphaFold Modeling

AlphaFold-multimer [31, 32], an AI-based program capable of predicting structures of multi-protein complexes based on the amino-acid sequences was used to predict interactions between human FABP4 (UniProt P15090) and extracellular cadherin domains (EC) of human DSG2 (UniProt Q14126). All calculations were performed at the University of Minnesota Super Computing institute (MSI) high-performance computing center using a non-Docker-based AlphaFold implementation model. AlphaFold calculations were subsequently performed on MSI's NVIDIA V100, and A100 GPU nodes. The highest ranked AlphaFold predictions for each set of interaction predictions were evaluated using PyMOL.

Generation of DSG2-silenced MCF-7 cells

The lentivirus-based RNA interference (RNAi) vector pLKO1 was used for siRNA-mediated DSG2 knockout in MCF-7 cells. siRNA transfection was performed using Lipofectamine 3000 (#L3000001, Invitrogen) according to the manufacturer's protocol. Recombinant lentiviruses were packaged in 293FT cells and harvested 48 hours post-transfection. Lentiviruses were then transduced into MCF-7 cells and after a 48 hr recovery, selected using 2 μg/mL puromycin. Stable knockdown cell lines were generated from a heterogeneous pool of puromycin-resistant MCF-7 cells and were cultured in DMEM supplemented with 5% FBS, 2 μg /mL insulin, 1 μg /mL puromycin and 1 mM penicillin-streptomycin in a humidified incubator at 37° C with 5% CO_2. The degree of silencing was evaluated using quantitative PCR and Western blotting.

ERK Phosphorylation Assays

MCF-7 cells were seeded in 6-well plates at a concentration of 2×10^5 cells/mL in media containing 5% FBS, 2 μg/mL insulin and 1 μg /mL puromycin. Cells were cultured for 24 hours and replaced with DMEM supplemented with 0.1% FBS. After 24 hours, cells were washed and treated with 20, 100 or 200 ng/mL FABP4 in DMEM supplemented with 0.1% FBS for the indicated times. Cells were lysed in RIPA buffer (50 mM Tris pH7.4, 150 mM NaCl, 0.1% SDS, 0.5 % sodium deoxycholate, 1% Triton-X100) with protease (#539134, Millipore) and phosphatase inhibitors (#P5726, #P0044, Millipore) and subject to Western blotting.

Co-immunoprecipitation

MCF-7 cells were lysed in extraction buffer (25 mM Tris, 150 mM NaCl, 1 mM EDTA, 1% NP-40, pH 7.4) containing the protease inhibitor cocktail Millipore #539134 and allowed to incubate at 4° C for 2 hours with gentle rotation. A detergent solubilized extract was obtained following centrifugation at 100,000g and used for immunoprecipitation. To immunoprecipitate the DSG2-FABP4 complex, 10μg of anti-DSG2 monoclonal antibody (sc80663, Santa Cruz) was bound to Dynabeads™ Protein G (#10003D, Invitrogen), pelleted by centrifugation, and washed with extraction buffer. Subsequently, the soluble cell lysate was incubated with antibody bound Dynabeads overnight at 4° C. Next, the DSG2-antibody bead complex was recovered by centrifugation, washed and incubated with 1μM FABP4 (pre-incubated with 10μM oleate) for 2 hours at 4° C. The protein-bead complex was

subsequently washed, and bound proteins eluted using 4% SDS. The composition of the eluted proteins was evaluated by Western blotting.

Glutathione S-transferase (GST) Pull-down Assays

GST-tagged FABP4 or R126Q (2 μM) was immobilized to glutathione-sepharose resin in the presence or absence of 20 μM oleate for 1 hour in wash buffer (50 mM Tris-HCl pH 7.4, 100 mM NaCl). The sample was pelleted by brief centrifugation at 500 × g and the unbound proteins removed by washing. 0.2 μM His-DSG2 EC3–4 (MBS2033234) was incubated with the resin with or without His-R126Q (0.2 μM, 2 μM, or 10 μM). The resin was then pelleted and washed as before. All steps above were performed at 4° C. The captured proteins were eluted by heating in SDS-PAGE sample loading buffer for 5 minutes and evaluated by immunoblotting.

Western Blot

Samples for analysis were separated using by 12% SDS-PAGE and transferred to a PVDF membrane (Bio-Rad) for Western blotting. After pre-incubation with blocking buffer (#927–60001, Li-Cor Biosciences), membranes were incubated with primary antibody overnight at 4° C followed by washing with 0.1% Tween-20 in phosphate-buffered saline 3 times and incubated with secondary antibody conjugated to Li-Cor IRDye for 1 hour and visualized using Odyssey infrared imaging (Li-Cor Biosciences). The primary antibodies used were DSG2 (ab150372, abcam; sc-80663, Santa Cruz), DSC1(sc-398590, Santa Cruz), DSC2(AF4688, R&D systems) and β-actin (A2228, Sigma). Antibodies against p44/p42 MAPK (ERK) (#9102), Phospho-p44/42 MAPK (ERK) (Thr202/Tyr204) (#9106), AKT (#9272), Phospho-Akt (Ser473) (#9271) and GADPH (#5174) were obtained from Cell Signaling Technology.

Statistical analysis

Values are reported as mean ± standard error (SEM) for figures and mean ± standard deviation (SD) for the text. Differences were compared using a Students' t-test or analysis of variance (ANOVA) with Sidak's post hoc multiple comparisons test. Survival was evaluating utilizing Kaplan-Meier method and log-rank tests. Statistical analyses were performed using GraphPad Prism version 7.0 (GraphPad Software, La Jolla, California, USA).

Data Availability

The data generated in this study are available within the article and its supplementary data files. Some raw data for this study were generated at the University of Minnesota Center for Mass Spectrometry and Proteomics. Derived data supporting the findings of this study are available from the corresponding author upon request.

RESULTS

eFABP4 has Proliferative Effects on MCF-7 Cells and T47D Breast Cancer Epithelial Cells.

Obesity is a positive risk factor for development of breast cancer and circulating levels of eFABP4 are increased ~5-fold as a function of elevated body mass [4, 9]. To address

mechanistic relationships between eFABP4 and progression of breast cancer, MCF-7 or T47D breast cancer cells that lack endogenous FABP4 were treated with eFABP4, and cell proliferation was assessed. MCF-7 and T47D breast cancer cell lines are classified as luminal A (ER+, PR+/−, HER2-) [33]. To assess the necessity of fatty acid binding in FABP4 effect, we utilized a non-fatty acid-binding mutant of FABP4, R126Q, to evaluate the contribution of FABP4's lipid binding to cellular proliferation in MCF-7 cells. The single residue substitution of glutamine for arginine of the R126Q mutant disrupts ion pairing between the carboxylate head group of the fatty acid and the basic side chain such that the affinity for FFA is reduced by over 100-fold [34].

Importantly, cell proliferation increased only with wild type recombinant eFABP4 but was not stimulated by the non-fatty acid binding FABP4 mutant R126Q in either MCF-7 (Figure 1A) or T47D cells (Figure 1C). Furthermore, increasing concentrations of eFABP4 present in the cell media (20, 100, and 200 ng/mL) resulted in significantly increased cell proliferation in a time and concentration dependent manner (Figure 1B). Additionally, the potentiation of proliferation was specific for eFABP4; FABP1 that adopts the same fold as FABP4 and binds fatty acids similarly [6], did not have any effect on MCF-7 cell growth (Figure 1E), indicating that fatty acid binding to FABP4 was essential to its function. Other phenotypic changes in cellular appearance such as cell size or shape were not affected by eFABP4.

FABP4 null mice restrict tumor growth and enhance survival.

Similarly, when E0771 cells were treated with varying concentrations of eFABP4 (20, 100, and 200 ng/mL) cell proliferation was increased in a time and concentration dependent manner (Figure 1D). Moreover, eFABP4 treatment at all concentrations modestly increased cell viability (~ 20%) under the same conditions (Supplementary Figure S2B). In vivo, using a high fat diet mouse model, growth of the murine breast cancer tumors was significantly delayed when E0771 cells were implanted into the FABP4 null mouse (designated as AKO) (Figure 2A) compared to implantation and tumor growth in wild type C57Bl/6J mice. This coincided with significantly potentiated overall survival in the AKO cohort (Figure 2B). AKO mice characteristically demonstrated a trend towards lower body weight and reduced body mass towards the end of the survival period.

eFABP4 activated the ERK-NRF2 pathways in MCF-7 cells.

The mitogen-activated protein kinases (MAPK) signaling plays an important role in cancer proliferation [35]. Activating mutation of this pathway, which is hallmarked by a high prevalence of BRAF and NRAS mutations, occurs in over 40% of all human cancers [36, 37]. The hyperactivation of MAPK contributes to constitutive ERK phosphorylation, resulting in potentiated cellular proliferation [38]. Treatment of MCF-7 cells with eFABP4 significantly increased the phosphorylated ERK (pERK) while R126Q did not (Figure 3A and 3B).

The NRF2 pathway is of primary importance in maintaining redox homeostasis. Under basal conditions, NRF2 is degraded in the cytoplasm via KEAP1 but in response to stressed conditions, NRF2 is activated and translocates to the nucleus and initiating the

transcription of various antioxidant genes thereby reducing reactive oxygen species (ROS) levels [39]. As an emerging concept, reductive stress is defined as a condition characterized by excess accumulation of reducing equivalents (e.g., NADH, NADPH, GSH), suppressing the activity of endogenous oxidoreductases. Recent studies show NRF2 as a controller of reductive stress [40] and NRF2 activation promotes cancer growth [41, 42], metastasis [43] and drug resistance [44, 45]. NRF2 is an ERK phosphorylation target [46–48] and the translocation of NRF2 to the nucleus is activated by ERK phosphorylation [49, 50] while ERK inhibitors attenuate NRF2 activity [51]. ERK/NRF2 signaling pathway has been reported to promote tumor growth in a variety of cancers [41, 52–54], protecting cancer cells from oxidative injury [52]. We used the antioxidant response element (ARE) luciferase reporter gene system and found that eFABP4 treatment resulted in significantly increased NRF2 transcriptional activation (Figure 3C). Aldehyde dehydrogenase 1 (ALDH1A1) is one of downstream antioxidant genes of NRF2, which catalyzes the irreversible oxidation of a wide range of aldehydes to their corresponding carboxylic acid and was linked to breast cancer invasiveness [55]. In line with the activation of NRF2, ALDH1A1 was upregulated about 2-fold following eFABP4 treatment (Figure 3D). Similarly, other NRF2 targets such as cytochrome P450 family 1 subfamily A member 1(CYP1A1), heme oxygenase 1(HMOX1) and superoxide dismutase 1 (SOD1) [56] were also upregulated specifically with eFABP4 but not R126Q. Accordingly, the downstream ROS level was significantly decreased in eFABP4 treated MCF-7 cells (Figure 3H). However, none of these effects were observed in R126Q-treated MCF-7 cells (Figure 3A–3H), indicating that fatty acid binding to FABP4 was essential to its function. As an alternate experimental strategy towards interrogation of NRF2 on MCF-7 growth, chemical inhibition of NRF2 with brusatol abrogated the proliferative effects of FABP4 in MCF-7 cells (Figure 3I). In aggregate, these results demonstrated that FABP4 stimulated MCF-7 growth through NRF2 signaling axis.

Proximity labeling of MCF-7 cells to identify a putative eFABP4 receptor.

Proximity labeling has been used successfully to identify intracellular and extracellular binding partners in a variety of contexts [57–59]. The experimental design makes use of fusion proteins between an experimental ligand (protein) and ascorbate peroxidase (APEX2) that when incubated with a suitable substrate and oxidant, produces a short-lived, diffusible radical that non-specifically adds to the side chains of proteins in a proximity-based manner. In our design we utilized biotin-that was disulfide linked to tyramide that when oxidized by ascorbate peroxidase in the presence of hydrogen peroxide produces a biotinylated phenoxyl radical. Avidin-based capture coupled with mass spectrometry analysis produces a protein dataset from which to interrogate functional interactions. To that end, we adopted an APEX2-FABP4 (along with APEX2 alone control) study design to identify putative eFABP4 binding partners.

Recombinant FABP isoforms (native and R126Q FABP4) were expressed in E. coli as His-tagged fusion proteins as previously described [34]. The purity of His-tagged recombinant proteins FABP4, APEX2 and APEX2-FABP4 is shown in Figure 4A. To assess the fatty acid binding affinity of recombinant proteins, we utilized the 1,8 ANS binding assays on the His-tagged fusions [60]. As shown in Figure 4B, APEX2-FABP4 and FABP4 exhibited the same lipid-binding activity while APEX2 was essentially devoid of any ligand binding.

Moreover, APEX2-FABP4 retained peroxidase activity that was qualitatively similar to that of APEX2 alone (Figure 4C).

APEX2-FABP4 and APEX2 control protein was added to MCF-7 cells in the presence of biotin S-S tyramide for 10 minutes and hydrogen peroxide added for 1 minute as an oxidant for the peroxidase activity. Following modification, the reaction was quenched, and the cells rapidly washed and lysed. Biotinylated proteins were captured using avidin-sepharose and proteins identified using mass spectrometry. There were 361 proteins identified using either APEX2 or APEX2-FABP4 treated MCF-7 cells and the results are presented as the ratio of ions detected by APEX2-FABP4 compared to that detected by APEX2 alone (Figure 5). Surprisingly, among the top APEX2-FABP4 captured proteins we identified several proteins functioning in desmosomes as potential FABP4 receptor candidates including desmoglein (DSG), desmocollin (DSC), junction plankoglobin (JUP), desomoplankin (DSP) and several cytokeratins (CK) (Figure 5).

Downregulation of desmosomal cadherins promote cancer progression.

Desmosomes are adhesive intercellular junctions that connect cells by desmosomal cadherins. Three major components of desmosome are desmosomal cadherins desmoglein and desmocollin, the armadillo family proteins plakoglobin and plakophilin, and the plakin family protein desmoplakin [61]. Keratin filaments interact with desmosomes to form networks subjacent to the membrane [62]. Importantly, our proximity labeling strategy identified over a dozen members of the desmosomal complex (Figure 5). Because the biotin-phenoxyl radical can diffuse after activation (even within the 1-minute labeling time frame), it is not unreasonable to identify several members of the desmosomal protein family given their close physical proximity. However, since the extracellular cadherin domains (EC) of DSG and DSC may be most likely to interact with eFABP4, we further analyzed these two classes of proteins in MCF-7 cells.

DSG and DSC are transmembrane proteins with five extracellular domains, a single-pass transmembrane domain, and a cytoplasmic domain. The five extracellular domains are composed of four extracellular cadherin repeats (EC1–4) and one extracellular anchor domain [63]. DSG and DSC isoforms are differentially expressed in epithelial cells while DSG2 and DSC2 are widely expressed in all desmosome-containing tissues [63] [64]. Previous studies have shown an association between desmosomal cadherins and cancers with reduced expression of desmosomal cadherins being observed in various tumors. In contrast, overexpression of desmosomal cadherins inhibit cancer progression [64]. Paradoxically, in MCF-7 cells, DSG2, DSC1 and DSC2 were detectable at both the mRNA (Supplementary Figure S1A–C) and protein level (Supplementary Figure S1D–G), while DSG isoforms 1, 3 or 4 were not immunologically detectable, despite being identified by mass spectrometry. Based on relative abundance in MCF-7 cells, we chose to focus on DSG2 for further analysis.

AlphaFold modeling predicted eFABP4 interaction with the ECs of DSG2.

Hypothesizing that desmosomal cadherins serve as FABP4 receptors to transduce intracellular signaling, we employed AphaFold to model FABP4 interaction with ECs of

desmosomal cadherin DSG2. AlphaFold is an artificial intelligence-based program that performs predictions of protein structure [65]. Two confidence measures were used to evaluate the reasonableness of AlphaFold predictions. One is a per-residue measure of local confidence termed predicted Local Distance Difference Test (pLDDT), while the second is Predicted Aligned Error (PAE), that reports AlphaFold's expected position error between individual alpha-carbons in the model. A consistently low PAE suggests AlphaFold is confident about the relative domain positions.

Modeling the interaction between FABP4 (UniProt P15090) and each individual EC (1 through 4) of DSG2 (UniProt P15090), AlphaFold predicted interactions (based on pLDDT and PAE metrics) between FABP4 and each EC, with the highest confidence values focused on EC3 and EC4 (Figure 6A). When AlphaFold was challenged with defining an interaction between FABP4 and an EC3-EC4 fusion, the prediction placed FABP4 onto EC3 (Figure 6B). Interestingly, structural modeling placed the orientation of EC3 onto a key proximal region of FABP4. This region is referred to as the "portal" and is characterized as the fatty acid ligand entry-exit site [6]. Within the portal region lie two determinants for fatty acid binding: helix alpha2 and the side chain of F57 (Figure 6C). The side chain of F57 affects ligand affinity, but not selectivity while helix alpha2 participates in protein-protein interaction with other lipid binding proteins such as the adipocyte hormone-sensitive lipase [66–68].

Co-immunoprecipitation and GST pull-down assays demonstrated the interaction between FABP4 and DSG2.

To corroborate the physical interaction between FABP4 and DSG2 identified by proximity labeling, we performed co-immunoprecipitation of FABP4 to DSG2 bound to Dynabeads. As shown in Figure 6D, His-FABP4 was co-immunoprecipitated with DSG2 detergent extracted from MCF-7 cells. To demonstrate that the interact was direct, GST pull-down assays using GST-FABP4 and His-DSG2 EC3–4 further confirmed direct interaction between eFABP4 and the EC3–4 region of DSG2 (Figure 6E, 6F). The DSG2-FABP4 interaction was potentiated in the presence of oleic acid (C18:1) (Figure 6E, 6F) and consistent with this, the non-fatty acid binding mutant FABP4 mutant, R126Q, exhibited reduced interaction with FABP4. In competition assays, high levels of R126Q could compete with lipid bound FABP4 on DSG2 (Figure 6E, 6F). These results in sum suggest a direct interaction between eFABP4 and DSG2 and that complex formation is potentiated by fatty acids.

eFABP4 mediated cell proliferation is abolished in DSG2 silenced MCF-7 cells.

To assess the functional role of desmosomal cadherins in eFABP4 mediated cell growth, we used an RNA silencing strategy to create MCF-7 cells with decreased expression of DSG2. Two stable DSG2 knockdown cell lines were generated (Figure 7A, 7B) and silencing of DSG2 had no effect on the cellular levels of DSC1 or DSC2 (Supplementary Figure S1H). Consistent with prior work on the effect of Desmoglein mutations and cancer ([64, 69], silencing of DSG2 resulted in increased cellular proliferation (Figure 7C). However, in such DSG2 silenced cell lines, the proliferative effect of eFABP4 was completely abolished

compared to control siRNA-transduced MCF-7 cells that retained eFABP4 stimulation (Figure 7C).

Consistent with the growth effects, while the basal level of pERK was significantly higher in DSG2 knockdown compared to control siRNA-transduced MCF-7 cells, eFABP4 failed to increase pERK levels further (Figure 7D and 7E). Similarly, while the basal level of ALDH1A1 mRNA was also significantly higher in DSG2 knockdown compared to control siRNA-transduced MCF-7 cells, there was no additional up-regulation of ALDH1A1 mRNA expression with eFABP4 treatment (Figure 7F). The efficiency of DSG2-silencing is shown in Supplementary Figure S1I. Addition of eFABP4 had no significant impact on the level of DSG2, DSC1 or DSC2 mRNA or protein expression in wild type MCF-7 cells (Supplementary Figure S1A). Taken together, these results point to DSG2 as a possible receptor for eFABP4 that stimulates breast cancer proliferation through the ERK/NRF2 pathway.

Discussion

Obesity is frequently associated with cancer progression and adipose tissue contributes to this process by producing metabolic, endocrine and paracrine factors that impact tumor growth. The proposed mechanisms, however, have been diverse and varied [22, 29, 30]. On one hand, fatty acids released by adipocyte lipolysis may fuel energy requirements for growth of certain cancers (e.g., ovarian) while alternatively, adipokines my potentiate tumorigenesis through endocrine or paracrine signaling. Of the various adipokines that may be tumor regulators, eFABP4, a lipid carrier, has received considerable attention. eFABP4 has been found to influence both tumor cell proliferation and in vivo tumor progression in a number of systems [22, 29]. Previous studies from our laboratory revealed that eFABP4 stimulated the proliferation of pancreatic cancer cells via activation of the NRF2 pathway [70] and the ERK/NRF2 signaling axis is reported to promote tumor growth in a variety of cancers [41, 52–54]. Our studies employing MCF-7 cell and in vivo in the FABP4 null mouse model suggested that eFABP4 treatment stimulated cell proliferation (Figure 1) and tumor progression (Figure 2) in breast cancer. More specifically, eFABP4 increased pERK level, activated NRF2 transcription, up-regulated expression of NRF2 downstream antioxidant genes ALDH1A1, CYP1A1, HMOX1 and SOD1 leading to reduced ROS levels (Figure 3). In addition, NRF2 inhibition abolished the proliferative effect of eFABP4 in MCF-7 cells (Figure 3F). These findings indicated that in MCF-7 cells, eFABP4 likely stimulates cell proliferation through the ERK/NRF2 signaling axis.

More than 90% of cancers originate from epithelial tissues [71]. Desmosomes are vital for the structure and function of cells in epithelial sheets, not only forming intercellular adhesion to ensure tissue integrity but also acting as signaling platforms involved in the regulation of cell proliferation, differentiation, migration, morphogenesis, and apoptosis [64, 69]. Dysfunction or destabilization of desmosome complexes is appreciated as a driver of cancer progression in multiple systems [69]. For example, in Wnt signaling, desmosome destabilization can provoke the release of JUP to activate oncogenic β-catenin signaling [72–74]. The MAPK pathway has also been identified as a potential system regulated by desmosomal proteins [75, 76]. ERK is normally kept inactive by its regulator Erbin.

Desmosomal cadherins DSGs or DSCs capture Erbin via their cytosolic domains thereby inhibiting ERK activation, whereas disruption of the DSC-DSG interaction or loss of DSCs or DSGs activates ERK signaling [75–77]. In our DSG2 knockdown MCF-7 cells, the basal level of pERK and ALDH1A1 mRNA were significantly higher than control siRNA-transduced cells (Figures 7D–F) leading to increased cell growth. Moreover, eFABP4 failed to potentiate cell proliferation, pERK level or ALDH1A1 mRNA expression in DSG2 silenced cells (Figures 7D–F).

Despite the various effects of eFABP4 on hepatocytes, pancreatic β-cells, macrophages, cardiomyocytes, vascular endothelial cells and cancer cells [22, 25–29], potential receptors for FABP4 have not been identified. In the current study, we utilized proximity labeling involving an APEX2-FABP4 fusion protein and identified desmosomal proteins including DSC, DSG, JUP, PKP and CK, as eFABP4 receptor candidates (Figure 5). Consistent with this proposition, Masana and colleagues previously reported that eFABP4 uptake by endothelial cells was dependent on cytokeratin 1 (CK1), as CK1 silenced cells showed significantly reduced uptake of eFABP4 and reduced activation of NRF2 [27, 74].

A major advance in analysis of eFABP4-DSG2 interaction was the introduction of AlphaFold modeling as a tool towards interaction prediction. We focused our modeling on the extracellular domains of DSG due to their known affect in mediating cellular adhesion via heterotypic association with DSC proteins and the availability of high-resolution crystal structures [78]. Molecular modeling suggested the interaction between FABP4 and ECs of DSG2, likely EC3, and GST pull-down assays demonstrated their direct interaction in vitro with a EC3-EC4 fusion protein (Figure 6) that was potentiated by oleic acid. Furthermore, loss of DSG2 completely abolished eFABP4 effects in MCF-7 cells (Figure 7). It is unknown if eFABP4 affects heterotypic association between DSG and DSC proteins, but a working model suggests that eFABP4 binding to DSG (and possibly DSC) would negatively regulate desmoglein-desmocollin association thereby potentiating ERK-dependent signaling.

AlphaFold predicts an interaction between FABP4 and the EC3 domain of Desmoglein 2 involving an F57 interface along with helix alpha2. Fatty acids bind to FABPs with their lipid carboxylate buried into a large water-filled central cavity and their omega methyl group oriented towards the protein surface. F57 is important for fatty acid binding to FABP4 as it undergoes a rotation of almost 180 degrees from an inward orientation to an outward orientation coincident with lipid binding [66, 79, 80]. Mutants of FABP4 that substitute amino acids with smaller side chains at position 57 exhibited reduced fatty acid affinity, but no change in selectivity suggesting that the bulky Phe side chain effectively serves to seal the lipid internally. Supplementary Figure S2A shows that the predicted orientation of the F57 side chain in EC1–4 is in the apo FABP4 form suggesting that upon fatty acid binding the F57 sidechain rotates into the outward position to possibly mediate interaction with DSG2. Consistent with this, GST-based pull-down assays revealed a robust increase in FABP4-DSG2 association in the presence of oleate (Figure 6E, 6F). The predicted inward orientation of F57 suggests that fatty acid binding to FABP4 may be a key determinant in its interaction with desmosomal cadherins and provide an explanation why R126Q failed to stimulate cancer growth.

FABP4 also forms a physical complex with the intracellular hormone-sensitive lipase (HSL) of adipocytes to mediate lipolysis of fatty acids [81]. FABP4 physically associates with HSL on the surface of intracellular lipid droplets and the interaction is mediated by two ion pairs forming a charged quartet, one involving D17 to R30 and the second D18 to K21 [68]. D17, D18 and K21 reside on helix alpha1 while R30 is on helix alpha2 and binding to HSL involves pair switching in which the FABP4 basic residues form ion pairs with corresponding acidic sidechains on HSL [68]. Fatty acids potentiate FABP4-HSL interaction as measured by titration microcalorimetry and the non-fatty acid binding mutant, R126Q does not associate with HSL to any measurable extent [81]. Inspection of the region of EC3 predicted to interact with helix alpha2 reveals a cluster of acidic amino acids (Glu-Val-Asp-Tyr-Glu-Glu^{344}) in close proximity. Future work will determine if such ion pairing exists between FABP4 and EC3.

In summary, our findings reveal DSG2 as a possible receptor for eFABP4 that stimulates breast cancer growth through an ERK/NRF2 signaling axis. Although our current studies emphasize DSG2, it should be stressed that proximity labeling suggested DSC1 may also be an FABP4 interaction target. Identification of a cluster of proteins involved in desmosomal biology implicates this complex as a critical element for FABP4 association and provides insight into the mechanism of eFABP4 as a driver of obesity-related cancers.

Supplementary Material

Refer to Web version on PubMed Central for supplementary material.

ACKNOWLEDGEMENTS

We would like to thank the University of Minnesota Center for Mass Spectrometry and Proteomics core for protein analysis and the members of the Bernlohr laboratory for discussion and advice. We would also like to thank Drs. Wendy Gordon and Robert Evans for assistance with preliminary AlphaFold modeling.

Supported by NIH DK053189 and the United States Department of Agriculture Experiment Station to DAB, by NIH T32 DK108733 to KW and NIH R21 DK122832 to SI.

ABBREVIATIONS

FABP	fatty acid binding protein
eFABP4	extracellular or circulating FABP4
ERK	extracellular signal-regulated kinase ½
pERK	phosphorylated ERK
NRF2	nuclear factor E2-related factor 2
ARE	antioxidant response element
AKO	FABP4 knockout or null
ALDH1A1	aldehyde dehydrogenase 1 family member A1, also known retinaldehyde dehydrogenase 1

DSG	desmoglein
DSC	desmocollin
1,8-ANS	1-anilinonaphthalene 8-sulfonic acid
EC	extracellular cadherin domain
ROS	reactive oxygen species
CYP1A1	cytochrome P450 family 1 subfamily A member 1
HMOX1	heme oxygenase 1
SOD1	superoxide Dismutase 1

REFERENCES

1. Wang YX, et al. , Friend or foe: Multiple roles of adipose tissue in cancer formation and progression. J Cell Physiol, 2019. 234(12): p. 21436–21449. [PubMed: 31054175]
2. Neuhouser ML, et al. , Overweight, Obesity, and Postmenopausal Invasive Breast Cancer Risk: A Secondary Analysis of the Women's Health Initiative Randomized Clinical Trials. JAMA Oncol, 2015. 1(5): p. 611–21. [PubMed: 26182172]
3. Chan DSM, et al. , Body mass index and survival in women with breast cancer-systematic literature review and meta-analysis of 82 follow-up studies. Ann Oncol, 2014. 25(10): p. 1901–1914. [PubMed: 24769692]
4. Calip GS, et al. , Metabolic syndrome and outcomes following early-stage breast cancer. Breast Cancer Res Treat, 2014. 148(2): p. 363–77. [PubMed: 25301086]
5. Amiri M, et al. , Diverse roles of fatty acid binding proteins (FABPs) in development and pathogenesis of cancers. Gene, 2018. 676: p. 171–183. [PubMed: 30021130]
6. Hotamisligil GS and Bernlohr DA, Metabolic functions of FABPs--mechanisms and therapeutic implications. Nat Rev Endocrinol, 2015. 11(10): p. 592–605. [PubMed: 26260145]
7. Furuhashi M, et al. , Fatty Acid-Binding Protein 4 (FABP4): Pathophysiological Insights and Potent Clinical Biomarker of Metabolic and Cardiovascular Diseases. Clin Med Insights Cardiol, 2014. 8(Suppl 3): p. 23–33.
8. Josephrajan A, et al. , Unconventional Secretion of Adipocyte Fatty Acid Binding Protein 4 Is Mediated By Autophagic Proteins in a Sirtuin-1-Dependent Manner. Diabetes, 2019. 68(9): p. 1767–1777. [PubMed: 31171562]
9. Terra X, et al. , FABP 4 is associated with inflammatory markers and metabolic syndrome in morbidly obese women. Eur J Endocrinol, 2011. 164(4): p. 539–47. [PubMed: 21257725]
10. Tso AW, et al. , Serum adipocyte fatty acid binding protein as a new biomarker predicting the development of type 2 diabetes: a 10-year prospective study in a Chinese cohort. Diabetes Care, 2007. 30(10): p. 2667–72. [PubMed: 17620449]
11. Cabré A, et al. , Fatty acid binding protein 4 is increased in metabolic syndrome and with thiazolidinedione treatment in diabetic patients. Atherosclerosis, 2007. 195(1): p. e150–8. [PubMed: 17553506]
12. Vural B, et al. , Presence of fatty-acid-binding protein 4 expression in human epicardial adipose tissue in metabolic syndrome. Cardiovasc Pathol, 2008. 17(6): p. 392–8. [PubMed: 18417367]
13. Balci MM, et al. , Serum levels of adipocyte fatty acid-binding protein are independently associated with left ventricular mass and myocardial performance index in obstructive sleep apnea syndrome. J Investig Med, 2012. 60(7): p. 1020–6.
14. Hobaus C, et al. , FABP4 and Cardiovascular Events in Peripheral Arterial Disease. Angiology, 2018. 69(5): p. 424–430. [PubMed: 28847153]

15. Gormez S, et al. , Relationships between visceral/subcutaneous adipose tissue FABP4 expression and coronary atherosclerosis in patients with metabolic syndrome. Cardiovasc Pathol, 2019. 46: p. 107192. [PubMed: 31927390]
16. Ge XN, et al. , FABP4 regulates eosinophil recruitment and activation in allergic airway inflammation. Am J Physiol Lung Cell Mol Physiol, 2018. 315(2): p. L227–L240. [PubMed: 29696987]
17. Erbay E, et al. , Reducing endoplasmic reticulum stress through a macrophage lipid chaperone alleviates atherosclerosis. Nat Med, 2009. 15(12): p. 1383–91. [PubMed: 19966778]
18. Tuncman G, et al. , A genetic variant at the fatty acid-binding protein aP2 locus reduces the risk for hypertriglyceridemia, type 2 diabetes, and cardiovascular disease. Proc Natl Acad Sci U S A, 2006. 103(18): p. 6970–5. [PubMed: 16641093]
19. Rodríguez-Calvo R, et al. , Fatty acid binding protein 4 (FABP4) as a potential biomarker reflecting myocardial lipid storage in type 2 diabetes. Metabolism, 2019. 96: p. 12–21. [PubMed: 30999003]
20. Hui X, et al. , Adipocyte fatty acid-binding protein modulates inflammatory responses in macrophages through a positive feedback loop involving c-Jun NH2-terminal kinases and activator protein-1. J Biol Chem, 2010. 285(14): p. 10273–80. [PubMed: 20145251]
21. Guaita-Esteruelas S, et al. , Adipose-Derived Fatty Acid-Binding Proteins Plasma Concentrations Are Increased in Breast Cancer Patients. Oncologist, 2017. 22(11): p. 1309–1315. [PubMed: 28701570]
22. Hao J, et al. , Circulating Adipose Fatty Acid Binding Protein Is a New Link Underlying Obesity-Associated Breast/Mammary Tumor Development. Cell Metab, 2018. 28(5): p. 689–705.e5. [PubMed: 30100196]
23. Cui Y, Song M, and Kim SY, Prognostic significance of fatty acid binding protein-4 in the invasive ductal carcinoma of the breast. Pathol Int, 2019. 69(2): p. 68–75. [PubMed: 30694572]
24. Hao J, et al. , Expression of Adipocyte/Macrophage Fatty Acid-Binding Protein in Tumor-Associated Macrophages Promotes Breast Cancer Progression. Cancer Res, 2018. 78(9): p. 2343–2355. [PubMed: 29437708]
25. Cao H, et al. , Adipocyte lipid chaperone AP2 is a secreted adipokine regulating hepatic glucose production. Cell Metab, 2013. 17(5): p. 768–78. [PubMed: 23663740]
26. Wu LE, et al. , Identification of fatty acid binding protein 4 as an adipokine that regulates insulin secretion during obesity. Mol Metab, 2014. 3(4): p. 465–73. [PubMed: 24944906]
27. Martínez-Micaelo N, et al. , Extracellular FABP4 uptake by endothelial cells is dependent on cytokeratin 1 expression. Biochim Biophys Acta Mol Cell Biol Lipids, 2019. 1864(3): p. 234–244. [PubMed: 30521939]
28. Zhou M, et al. , Deficiency of adipocyte fatty-acid-binding protein alleviates myocardial ischaemia/reperfusion injury and diabetes-induced cardiac dysfunction. Clin Sci (Lond), 2015. 129(7): p. 547–59. [PubMed: 26186740]
29. Guaita-Esteruelas S, et al. , Exogenous FABP4 increases breast cancer cell proliferation and activates the expression of fatty acid transport proteins. Mol Carcinog, 2017. 56(1): p. 208–217. [PubMed: 27061264]
30. Nieman KM, et al. , Adipocytes promote ovarian cancer metastasis and provide energy for rapid tumor growth. Nat Med, 2011. 17(11): p. 1498–503. [PubMed: 22037646]
31. Gao M, et al. , AF2Complex predicts direct physical interactions in multimeric proteins with deep learning. Nat Commun, 2022. 13(1): p. 1744. [PubMed: 35365655]
32. Evans R, et al., 2022.
33. Dai X, et al. , Breast Cancer Cell Line Classification and Its Relevance with Breast Tumor Subtyping. J Cancer, 2017. 8(16): p. 3131–3141. [PubMed: 29158785]
34. Hertzel AV, et al. , Identification and characterization of a small molecule inhibitor of Fatty Acid binding proteins. J Med Chem, 2009. 52(19): p. 6024–31. [PubMed: 19754198]
35. Braicu C, et al. , A Comprehensive Review on MAPK: A Promising Therapeutic Target in Cancer. Cancers (Basel), 2019. 11(10).
36. Lee S, Rauch J, and Kolch W, Targeting MAPK Signaling in Cancer: Mechanisms of Drug Resistance and Sensitivity. Int J Mol Sci, 2020. 21(3).

37. Samatar AA and Poulikakos PI, Targeting RAS-ERK signalling in cancer: promises and challenges. Nat Rev Drug Discov, 2014. 13(12): p. 928–42. [PubMed: 25435214]
38. Yuan J, et al. , The MAPK and AMPK signalings: interplay and implication in targeted cancer therapy. J Hematol Oncol, 2020. 13(1): p. 113. [PubMed: 32807225]
39. Wu S, Lu H, and Bai Y, Nrf2 in cancers: A double-edged sword. Cancer Med, 2019. 8(5): p. 2252–2267. [PubMed: 30929309]
40. Xiao W and Loscalzo J, Metabolic Responses to Reductive Stress. Antioxid Redox Signal, 2020. 32(18): p. 1330–1347. [PubMed: 31218894]
41. Satoh H, et al. , Nrf2 prevents initiation but accelerates progression through the Kras signaling pathway during lung carcinogenesis. Cancer Res, 2013. 73(13): p. 4158–68. [PubMed: 23610445]
42. Rojo de la Vega M, Chapman E, and Zhang DD, NRF2 and the Hallmarks of Cancer. Cancer Cell, 2018. 34(1): p. 21–43. [PubMed: 29731393]
43. Wang H, et al. , NRF2 activation by antioxidant antidiabetic agents accelerates tumor metastasis. Sci Transl Med, 2016. 8(334): p. 334ra51.
44. Xue D, Zhou X, and Qiu J, Emerging role of NRF2 in ROS-mediated tumor chemoresistance. Biomed Pharmacother, 2020. 131: p. 110676. [PubMed: 32858502]
45. Singh A, et al. , Dysfunctional KEAP1-NRF2 interaction in non-small-cell lung cancer. PLoS Med, 2006. 3(10): p. e420. [PubMed: 17020408]
46. Yusuf IO, et al. , Fibroblast growth factor 9 activates anti-oxidative functions of Nrf2 through ERK signalling in striatal cell models of Huntington's disease. Free Radic Biol Med, 2019. 130: p. 256–266. [PubMed: 30391672]
47. Yang YC, et al. , Induction of glutathione synthesis and heme oxygenase 1 by the flavonoids butein and phloretin is mediated through the ERK/Nrf2 pathway and protects against oxidative stress. Free Radic Biol Med, 2011. 51(11): p. 2073–81. [PubMed: 21964506]
48. Jasek-Gajda E, et al. , Targeting the MAPK/ERK and PI3K/AKT Signaling Pathways Affects NRF2, Trx and GSH Antioxidant Systems in Leukemia Cells. Antioxidants (Basel), 2020. 9(7).
49. Madduma Hewage SRK, et al. , Galangin Activates the ERK/AKT-Driven Nrf2 Signaling Pathway to Increase the Level of Reduced Glutathione in Human Keratinocytes. Biomol Ther (Seoul), 2017. 25(4): p. 427–433. [PubMed: 27829272]
50. Kim JK and Jang HD, Nrf2-mediated HO-1 induction coupled with the ERK signaling pathway contributes to indirect antioxidant capacity of caffeic acid phenethyl ester in HepG2 cells. Int J Mol Sci, 2014. 15(7): p. 12149–65. [PubMed: 25007817]
51. Park JY, et al. , Morin Induces Heme Oxygenase-1 via ERK-Nrf2 Signaling Pathway. J Cancer Prev, 2013. 18(3): p. 249–56. [PubMed: 25337552]
52. Liang C, et al. , PIN1 Maintains Redox Balance via the c-Myc/NRF2 Axis to Counteract Kras-Induced Mitochondrial Respiratory Injury in Pancreatic Cancer Cells. Cancer Res, 2019. 79(1): p. 133–145. [PubMed: 30355620]
53. Hao Q, et al. , Sulforaphane suppresses carcinogenesis of colorectal cancer through the ERK/Nrf2-UDP glucuronosyltransferase 1A metabolic axis activation. Oncol Rep, 2020. 43(4): p. 1067–1080. [PubMed: 32323779]
54. Yang Y, et al. , NQO1 promotes an aggressive phenotype in hepatocellular carcinoma via amplifying ERK-NRF2 signaling. Cancer Sci, 2021. 112(2): p. 641–654. [PubMed: 33222332]
55. Khoury T, et al. , Aldehyde dehydrogenase 1A1 expression in breast cancer is associated with stage, triple negativity, and outcome to neoadjuvant chemotherapy. Mod Pathol, 2012. 25(3): p. 388–97. [PubMed: 22080062]
56. Ma Q, Role of nrf2 in oxidative stress and toxicity. Annu Rev Pharmacol Toxicol, 2013. 53: p. 401–26. [PubMed: 23294312]
57. Hung V, et al. , Spatially resolved proteomic mapping in living cells with the engineered peroxidase APEX2. Nat Protoc, 2016. 11(3): p. 456–75. [PubMed: 26866790]
58. Lobingier BT, et al. , An Approach to Spatiotemporally Resolve Protein Interaction Networks in Living Cells. Cell, 2017. 169(2): p. 350–360 e12. [PubMed: 28388416]
59. Lam SS, et al. , Directed evolution of APEX2 for electron microscopy and proximity labeling. Nat Methods, 2015. 12(1): p. 51–4. [PubMed: 25419960]

60. Kane CD and Bernlohr DA, A simple assay for intracellular lipid-binding proteins using displacement of 1-anilinonaphthalene 8-sulfonic acid. Anal Biochem, 1996. 233(2): p. 197–204. [PubMed: 8789718]
61. Dubash AD and Green KJ, Desmosomes. Curr Biol, 2011. 21(14): p. R529–31. [PubMed: 21783027]
62. Hatzfeld M, Keil R, and Magin TM, Desmosomes and Intermediate Filaments: Their Consequences for Tissue Mechanics. Cold Spring Harb Perspect Biol, 2017. 9(6).
63. Kowalczyk AP and Green KJ, Structure, function, and regulation of desmosomes. Prog Mol Biol Transl Sci, 2013. 116: p. 95–118. [PubMed: 23481192]
64. Huber O and Petersen I, 150th Anniversary Series: Desmosomes and the Hallmarks of Cancer. Cell Commun Adhes, 2015. 22(1): p. 15–28. [PubMed: 26133535]
65. Jumper J, et al. , Highly accurate protein structure prediction with AlphaFold. Nature, 2021. 596(7873): p. 583–589. [PubMed: 34265844]
66. Jenkins AE, et al. , Testing of the portal hypothesis: analysis of a V32G, F57G, K58G mutant of the fatty acid binding protein of the murine adipocyte. Biochemistry, 2002. 41(6): p. 2022–7. [PubMed: 11827549]
67. Gillilan RE, Ayers SD, and Noy N, Structural basis for activation of fatty acid-binding protein 4. J Mol Biol, 2007. 372(5): p. 1246–60. [PubMed: 17761196]
68. Smith AJ, et al. , Mapping of the hormone-sensitive lipase binding site on the adipocyte fatty acid-binding protein (AFABP). Identification of the charge quartet on the AFABP/aP2 helix-turn-helix domain. J Biol Chem, 2008. 283(48): p. 33536–43. [PubMed: 18820256]
69. Dusek RL and Attardi LD, Desmosomes: new perpetrators in tumour suppression. Nat Rev Cancer, 2011. 11(5): p. 317–23. [PubMed: 21508970]
70. Wirth K, et al. , Fatty acid binding protein 4 regulates pancreatic cancer cell proliferation via activation of nuclear factor E2-related factor 2. Surg Obes Relat Dis, 2022. 18(4): p. 485–493. [PubMed: 34998697]
71. Frank SA, Dynamics of Cancer: Incidence, Inheritance, and Evolution. 2007.
72. Klymkowsky MW, et al. , Membrane-anchored plakoglobins have multiple mechanisms of action in Wnt signaling. Mol Biol Cell, 1999. 10(10): p. 3151–69. [PubMed: 10512857]
73. Miller JR and Moon RT, Analysis of the signaling activities of localization mutants of beta-catenin during axis specification in Xenopus. J Cell Biol, 1997. 139(1): p. 229–43. [PubMed: 9314542]
74. Zhurinsky J, Shtutman M, and Ben-Ze'ev A, Plakoglobin and beta-catenin: protein interactions, regulation and biological roles. J Cell Sci, 2000. 113 (Pt 18): p. 3127–39. [PubMed: 10954412]
75. Cui T, et al. , The p53 target gene desmocollin 3 acts as a novel tumor suppressor through inhibiting EGFR/ERK pathway in human lung cancer. Carcinogenesis, 2012. 33(12): p. 2326–33. [PubMed: 22941060]
76. Harmon RM, et al. , Desmoglein-1/Erbin interaction suppresses ERK activation to support epidermal differentiation. J Clin Invest, 2013. 123(4): p. 1556–70. [PubMed: 23524970]
77. Berkowitz P, et al. , Desmosome signaling. Inhibition of p38MAPK prevents pemphigus vulgaris IgG-induced cytoskeleton reorganization. J Biol Chem, 2005. 280(25): p. 23778–84. [PubMed: 15840580]
78. Harrison OJ, et al. , Structural basis of adhesive binding by desmocollins and desmogleins. Proc Natl Acad Sci U S A, 2016. 113(26): p. 7160–5. [PubMed: 27298358]
79. Ory J, et al. , Biochemical and crystallographic analyses of a portal mutant of the adipocyte lipid-binding protein. J Biol Chem, 1997. 272(15): p. 9793–801. [PubMed: 9092513]
80. Simpson MA and Bernlohr DA, Analysis of a series of phenylalanine 57 mutants of the adipocyte lipid-binding protein. Biochemistry, 1998. 37(31): p. 10980–6. [PubMed: 9692991]
81. Jenkins-Kruchten AE, et al. , Fatty acid-binding protein-hormone-sensitive lipase interaction. Fatty acid dependence on binding. J Biol Chem, 2003. 278(48): p. 47636–43. [PubMed: 13129924]

IMPLICATIONS

These results suggest desmosomal proteins, and in particular Desmoglein 2, may function as receptors of eFABP4 and provide new insight into the development and progression of obesity-associated cancers.

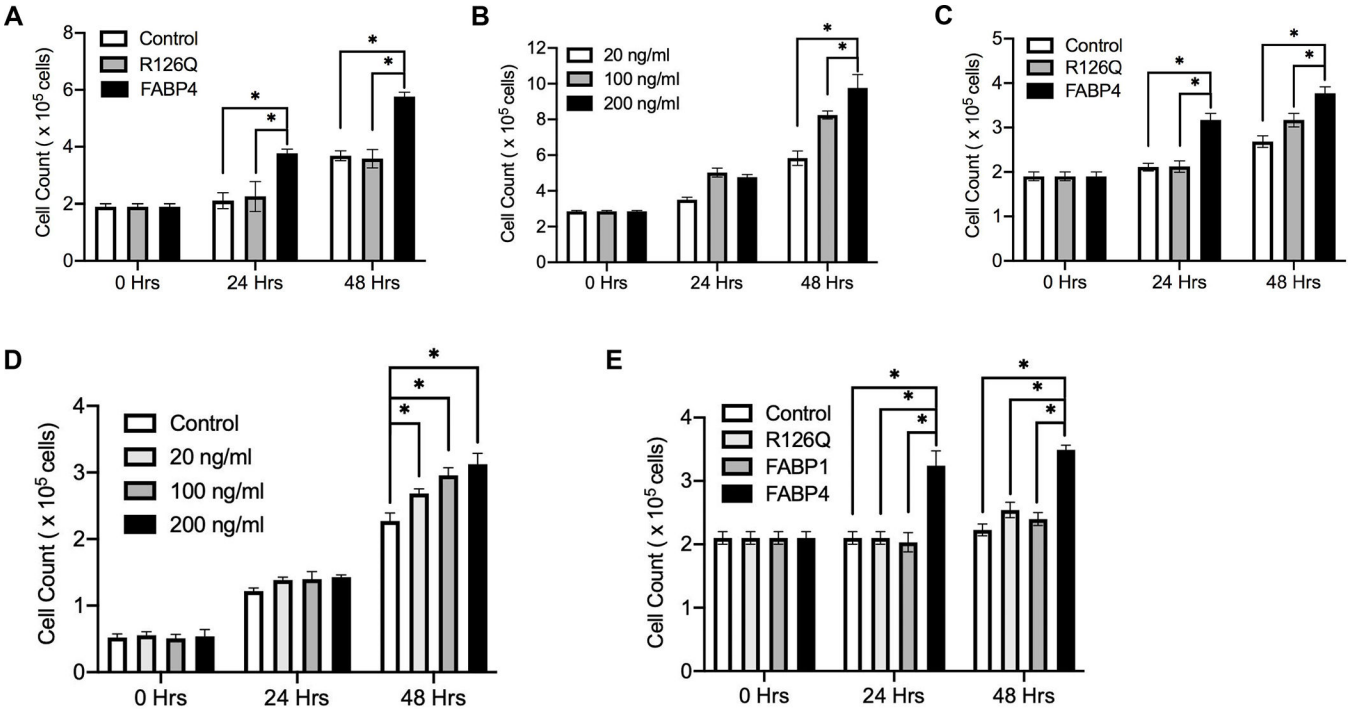

Figure 1. Proliferative effects of eFABP4 on breast cancer cell culture.

A) Effect of FABP4 or mutant R126Q on MCF-7 proliferation. B) Effect of varying concentrations and time of eFABP4 on MCF-7 proliferation. C) Effect of FABP4 or mutant R126Q on T47D proliferation. D) Growth of E0771 cells in response to varying concentrations of eFABP4. E) Effect of FABP1 compared to FABP4 and R126Q on MCF-7 cell growth. Results are shown for one experiment that was repeated 3 times. *, $p < 0.05$.

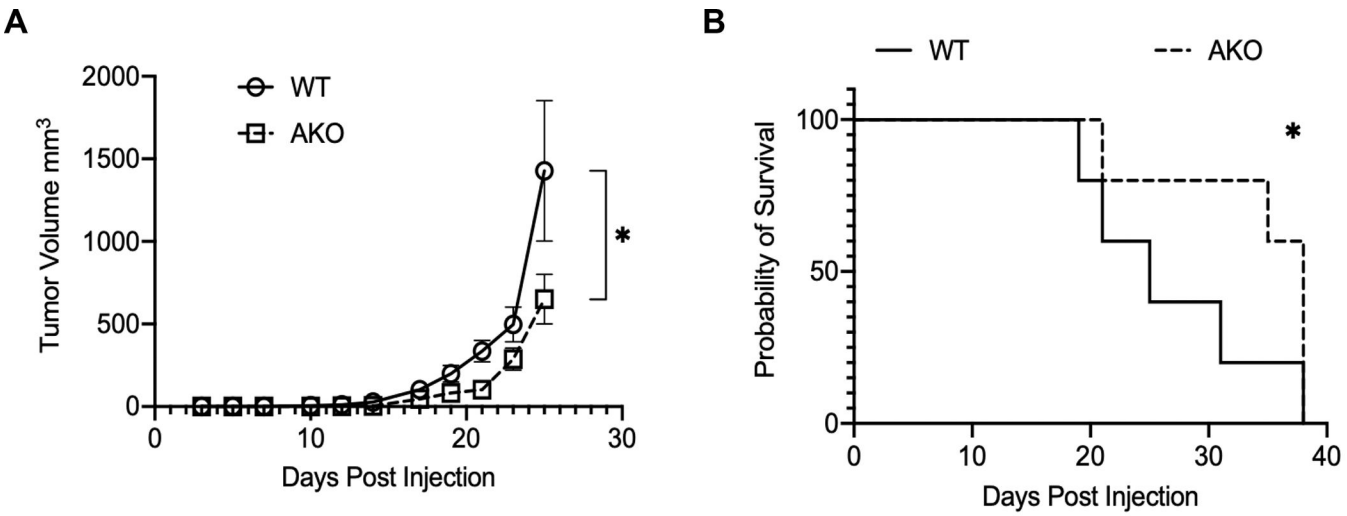

Figure 2. FABP4 null (AKO) mice injected with E0771 murine breast cancer showed decreased tumor volume and enhanced survival.

A) Tumor volume over time. B) Survival curves of FABP4 −/− null (AKO) mice vs. wild type (WT) mice. N = 20, 10 per group. *, $p < 0.05$.

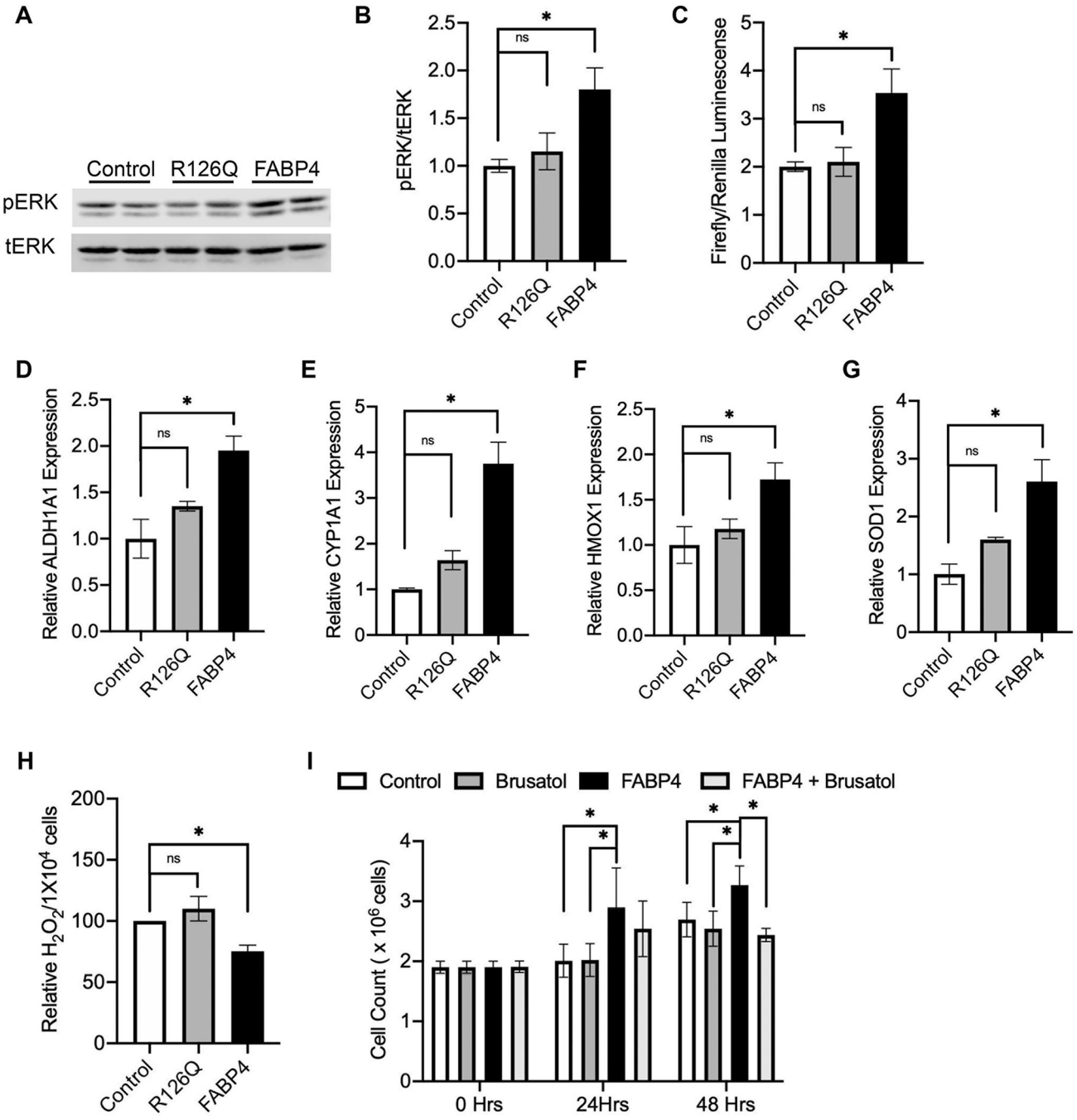

Figure 3. FABP4 mediated breast cancer growth was dependent on the ERK/NRF2 pathway.

A) MCF-7 cells were treated with 100 ng/mL FABP4 or R126Q for 5 minutes and pERK levels were evaluated using western blot. B) Quantification of pERK level in A). Bands of pERK were normalized to the level of tERK in the same samples. C) MCF-7 cells were treated with 100 ng/mL FABP4 or 100 ng/mL R126Q for 48 hours and the NRF2 activity was evaluated using the antioxidant response element (ARE) luciferase reporter gene system. D-G) mRNA expression of ALDH1A1, CYP1A1, HMOX1, and SOD1 were evaluated using qRT-PCR (normalized to TBP) following treatment of MCF-7 cells with 100

ng/mL FABP4 or 100 ng/mL R126Q for 48 hours. H) Levels of H_2O_2 were measured following treatment with 100 ng/mL FABP4 for 48 hours in MCF-7 cells. I) MCF-7 proliferation after chemical inhibition of NRF2 with 20 nM brusatol. Results are shown for one experiment that was repeated 3 times. *, $p < 0.05$. ns, nonsignificant.

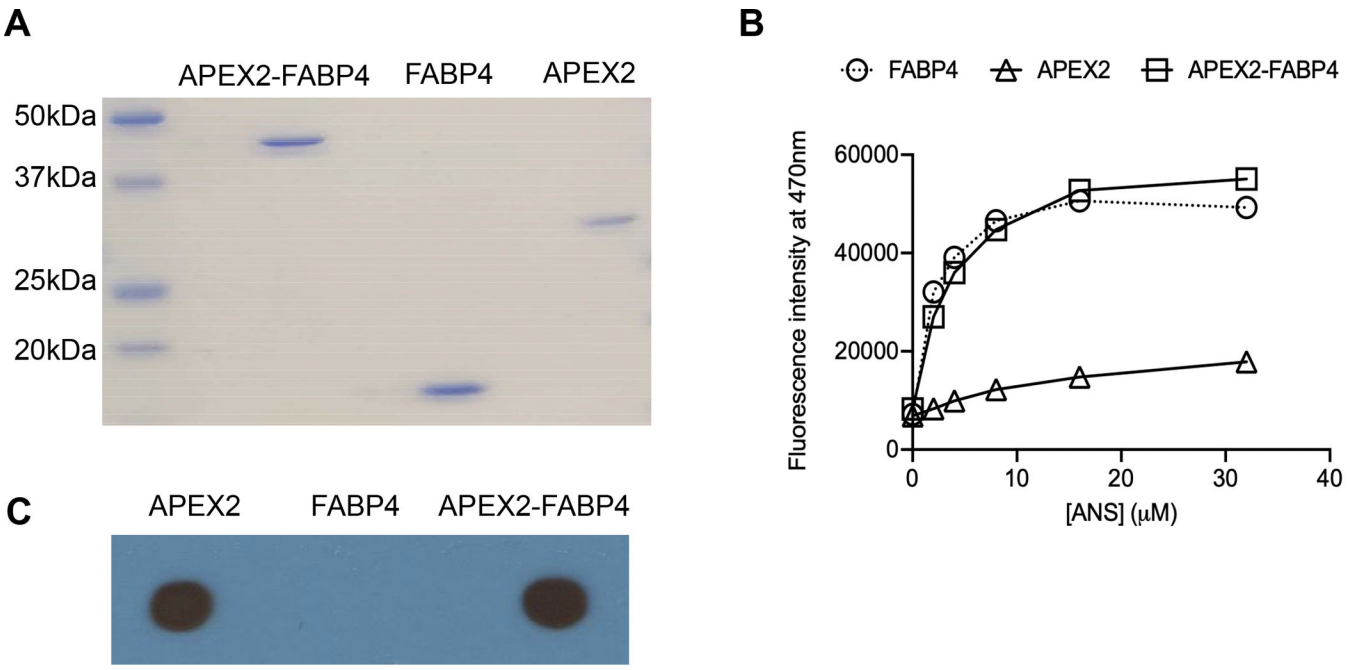

Figure 4. Recombinant protein APEX2-FABP4 was highly functional.

A) Recombinant proteins APEX2-FABP4, FABP4 and APEX2 expressed in E. coli were analyzed by SDS-PAGE stained with Coomassie blue. B) Fatty acid binding affinity of recombinant proteins was assessed with ANS binding assay. (C) Peroxidase activity of recombinant proteins were detected with luminol-based enhanced-chemiluminescence of HRP substrate.

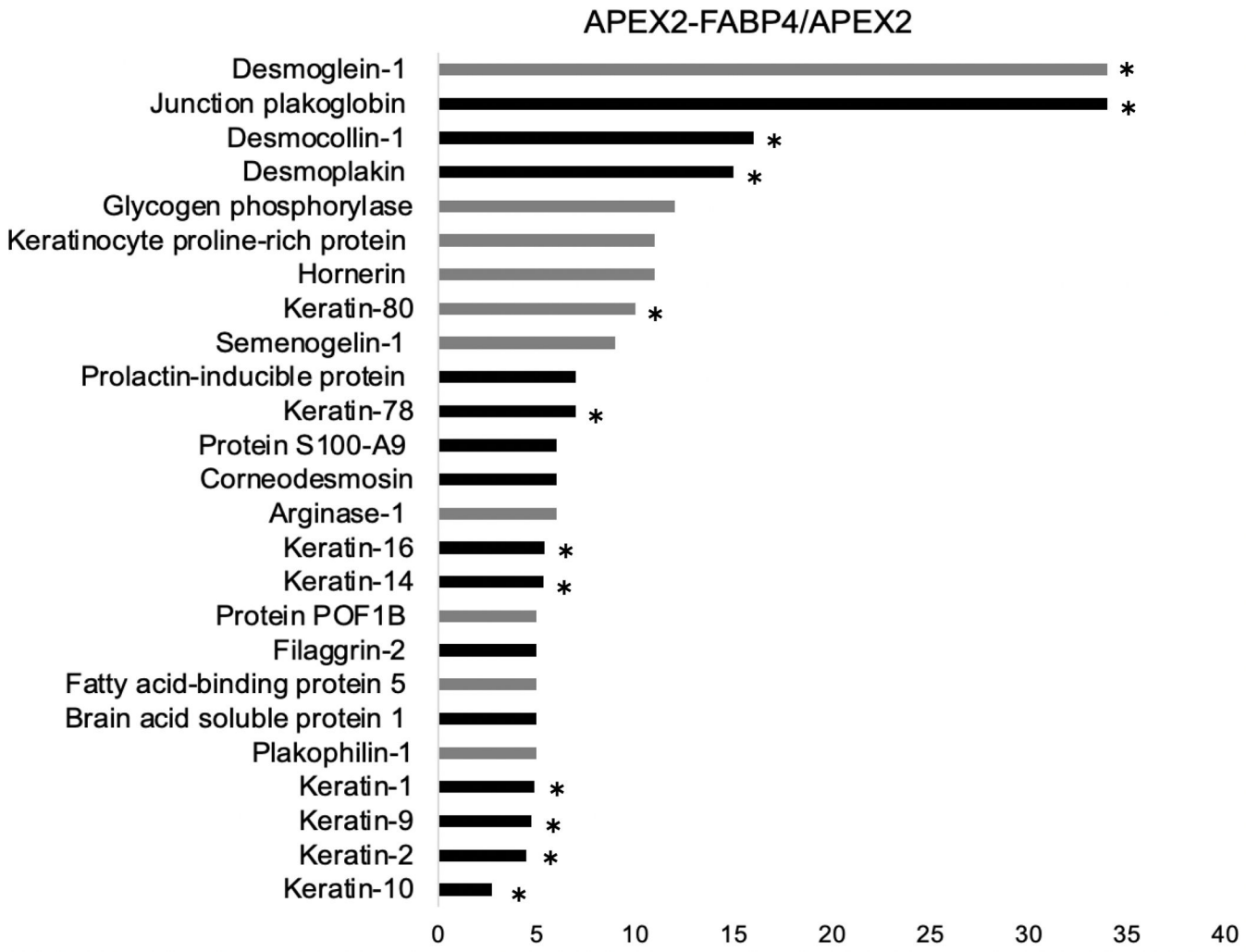

Figure 5. Top FABP4 receptor candidates identified by proximal labeling.

MCF-7 cells were treated with biotin-SS-phenol and APEX2-FABP4 or APEX2 followed by H_2O_2 to initiate biotin labeling. The biotinylated proteins were enriched using streptavidin magnetic and analyzed by mass spectrometry. The top FABP4 receptor candidates reported in mass spectrometry was normalized to APEX2. Bars in grey mean the output was "0" in APEX2 but put in "1" instead for normalization calculation. Asterisks showing the candidates are components of desmosome complex.

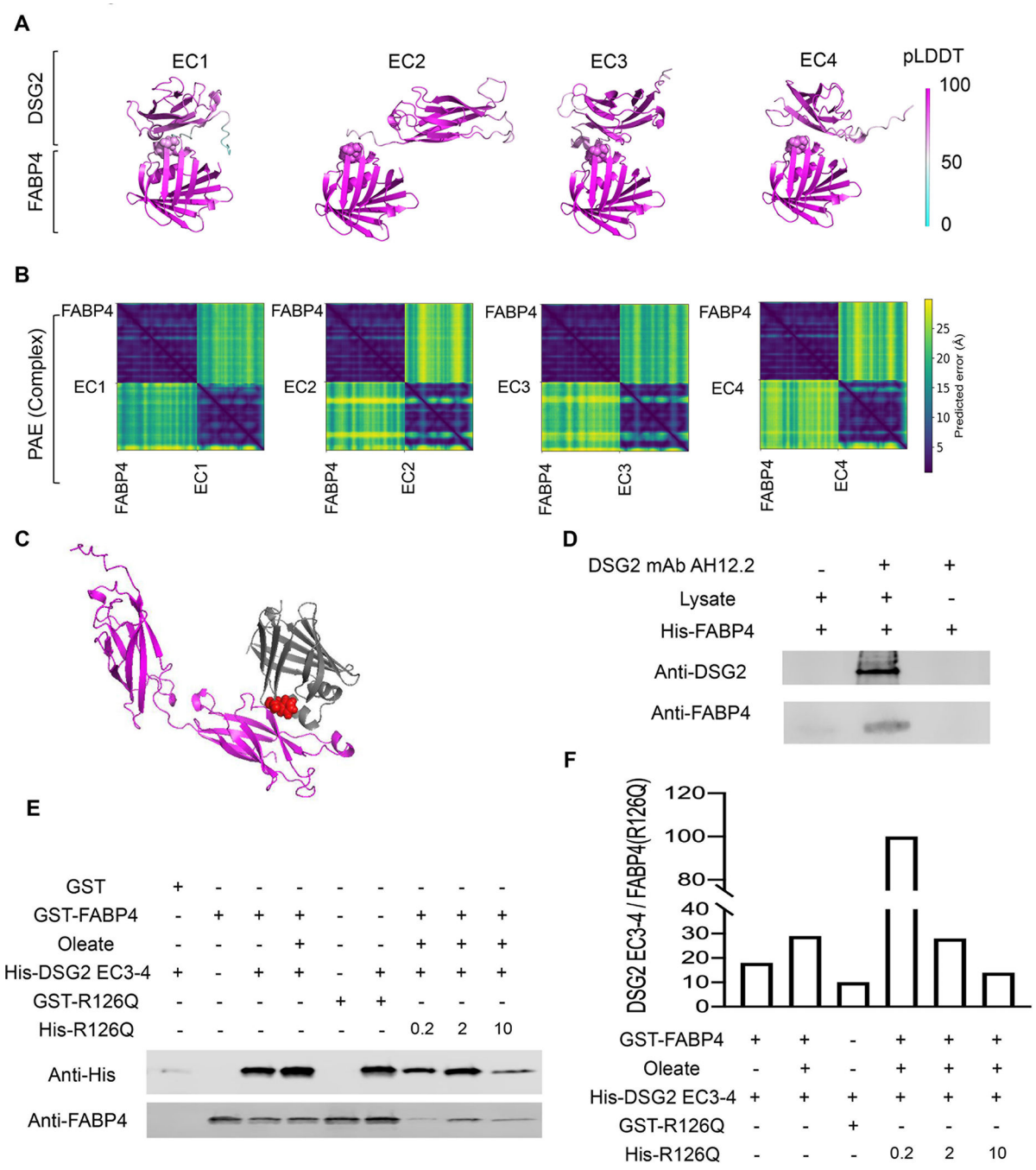

Figure 6. FABP4 interacted with ECs of DSG2.

A) AlphaFold predicted the interaction between FABP4 and each EC (1 through 4) of DSG2 individually. Top panel shows ribbon cartoons of the complex colored by AlphaFold's pLDDT parameter. Each residue in the sequence is color-coded based on the model confidence score. Model confidence from high to low: magenta (100), white (50), cyan (0). B) PAE distance plots show the distance error map. Blue is 0 angstroms error, yellow is 30 angstroms error. C) Docking of F57 (red) of FABP4 (grey) and DSG2 EC3–4 (magenta). The native structures of FABP4 (grey), and DSG2 EC3–4(magenta) are represented as

ribbons. D) MCF-7 cell lysates were incubated with DSG2 antibody bound Dynabeads as described in Methods 1μM FABP4 (pre-incubated with 10 μM oleate) was added to the protein-beads complex for 2 hr. and complexed proteins captured by centrifugation. Proteins in the FABP4-DSG2 complex were eluted and evaluated by immunoblotting. E) GST-tagged FABP4 or R126Q was immobilized to glutathione resin in the presence or absence of 20 μM oleate followed by incubation with 0.2 μM His-DSG2 EC3–4. Immunoblotting was performed to analyze the eluted proteins after incubation. F) Quantification of the results from panel E where the level of DSG2 EC3–4 was normalized to GST-FABP4 or GST-R126Q.

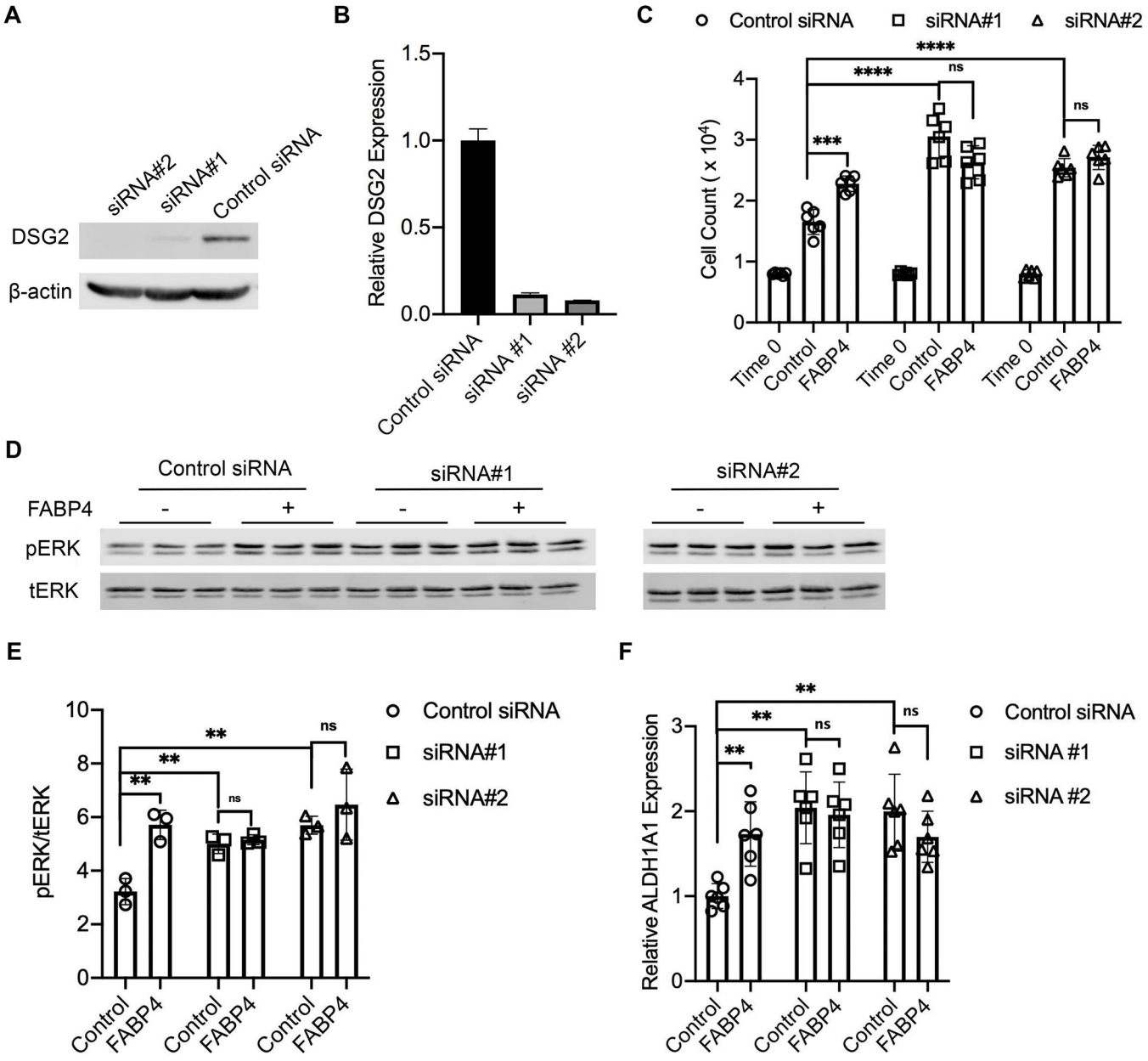

Figure 7. Loss of DSG2 abolished FABP4 mediated cell proliferation through ERK/NRF2 pathway in MCF-7 cells.

A) Two DSG2 knockdown (DSG2 siRNA#1 and DSG2 siRNA#2) MCF-7 cell lines were made. B) mRNA level of DSG2 expression in two DSG2 knockdown cells lines. C) Cells with stable knockdown of DSG2 were treated were treated with 200 ng/mL FABP4 for 48 hours and cell numbers were detected using CyQUANT Cell Proliferation Assay Kit. D) DSG2 knockdown cells were treated with 200 ng/mL FABP4 for 5 minutes and pERK level was evaluated using western blot. E) Quantification of pERK level in D). F) Cells with stable knockdown of DSG2 were treated with 200 ng/mL FABP4 for 48 hours and mRNA

expression level of ALDH1A1 was evaluated using qRT-PCR. **, $P < 0.01$; ***, $P < 0.001$; ****, $P < 0.0001$; ns, nonsignificant.